Reprinted from SPIE Vol. 238—Image Processing for Missile Guidance


# Use of thermal-inertia properties for material identification

**John P. Schieldge, Anne B. Kahle, Ronald E. Alley, Alan R. Gillespie**
Jet Propulsion Laboratory, California Institute of Technology
MS 183-501, 4800 Oak Grove Drive, Pasadena, California 91103

## Abstract

A knowledge of the thermal inertia of the Earth's surface can be used in geologic mapping as a complement to surface reflectance data as provided by Landsat. Thermal inertia, a body property, cannot be determined directly but can be inferred from radiation temperature measurements made at various times in the diurnal heating cycle, combined with a model of the surface heating processes. We have developed such a model and applied it along with temperature measurements made in the field and from satellite to determine thermal properties of surface materials. An example from a test site in western Nevada is used to illustrate the utility of this technique.

## Introduction

Thermal inertia (P) is a scalar quantity that provides a measure of a material's ability to resist a change in temperature. Furthermore, it depends upon volumetric, rather than surficial, properties of the material. Specifically, it is related to the material's density ($\rho$), specific heat capacity (c), and thermal conductivity (K) by the relationship,

$$P = (K\rho c)^{1/2}, \qquad (1)$$

which obtains for a homogeneous medium. It is this dependence upon volumetric properties that makes P a useful parameter in remote sensing applications. This is particularly so in geologic studies (such as lithologic mapping) where the surface -- as a result of weathering, staining, or other processes -- is often unrepresentative of the entire material. Then, if remote sensing methods relying solely upon surface reflectivity measurements are used, the task of discriminating among different materials becomes inordinately difficult. To facilitate identification, it is possible to make thermal inertia images of the Earth's surface to complement other remote sensing data.[1]

Thermal inertia cannot be measured directly. Instead, it can be inferred from the diurnal variation of temperature at the Earth's surface. The temperature regime at the surface depends not only upon the thermal inertia of the geologic material, but also upon many, complicated surface heating processes, such as latent and sensible heat transfer between ground and air. Therefore, determining P from the temperature data requires the use of mathematical modelling techniques.[2,3,4] This is not an easy task because it involves the solution of a partial differential equation of parabolic form whose upper (surface) boundary condition is inherently non-linear, and this usually restricts the method of solution to various finite difference techniques [5,6] in which one must exercise great care in ensuring the stability and convergence of the solutions. In remote sensing applications, the important parameter in determining P is the diurnal temperature range, $\Delta T = T_{maximum} - T_{minimum}$. $\Delta T$ data sets can be obtained from satellite or aircraft surveys of the thermal infrared (IR) emission of the Earth's surface at 8 - 14 μm. A thermal model of heat flow in the surface layers can then be used to predict $\Delta T$ as a function of thermal inertia; P can be extracted from the actual $\Delta T$, provided the surface boundary conditions are estimated accurately.

In this paper, we have presented the results of a study whose purpose was to produce a detailed thermal inertia image, from satellite and ground-truth data, of a region of western Nevada. The data were collected in July, 1978. Visible and infrared data were obtained from the Heat Capacity Mapping Mission (HCMM) satellite. HCMM is equipped with a scanning radiometer with two channels: one bandwidth at 0.5 - 1.1 μm and another at 10.5 - 12.5 μm.[7] The satellite passed over the Nevada area twice consecutively, in the predawn and afternoon hours of the 22nd. Concurrently a JPL team collected ground-truth data, at selected locations over the test site, of surface and subsurface temperatures, and local meteorological conditions. These data were used in the JPL thermal model, developed by Kahle [6]; then, the results were processed by a technique developed to construct digital images of thermal inertia in the form of photographic facsimiles.[8] The details follow below.

## Thermal Model for Computation of Thermal Inertia

Subject to a specific set of boundary conditions, the JPL thermal model is used to compute the surface-subsurface temperature profile as a function of time. The basis for the model is the one-dimensional heat conduction equation,

$$\frac{\partial T}{\partial t} = \kappa \frac{\partial^2 T}{\partial Z^2}, \tag{2}$$

where T is temperature, t is time, Z is depth, and $\kappa$ is thermal diffusivity (= $K/\rho c$). It is assumed that the heat flux density at the lower boundary, Z = 0.5 m, is negligible over a diurnal cycle. At the upper (surface) boundary, the net heat flux density is zero,

$$S + R + H + L + G = 0 \tag{3}$$

Here, S is net solar radiation; R is net thermal radiation from ground and air; H is sensible heat transfer between ground and air; L is latent heat transfer between ground and air; G is heat flux density in the ground.

The solution of equation (2) is critically dependent upon the solution of equation (3), particularly the parameterization of S, R, H, L, G. Complete details of the parameterizations are given elsewhere;[6] briefly, a simple approach to these computations has been adopted. In particular, L is usually, but not always, negligible in arid regions. Therefore, we have omitted it from our computations, and employ in our analysis a so-called dry model. The other terms in (3) are described as follows.

Values of S are obtained from a formulation developed by Joseph [9] and Arakawa et al. [10]. S includes not only direct solar insolation but also solar radiation diffusely scattered by the atmosphere. The formulation is applicable to cloudy or cloudless conditions and also accounts for atmospheric absorption, water vapor content of the atmosphere, topography, and ground albedo. Most of these factors can be determined from in situ observations; the ground albedo, on the other hand, can be obtained by satellite or aircraft survey.

Thermal radiation, R, is emitted by the sky and ground. For simplicity, both mediums are considered to be blackbody radiators so that they are quartic functions of temperature, i.e. $\sigma T^4$, where $\sigma$ is the Stefan-Boltzman constant. For the sky, an effective temperature is used according to the empirical formulation of Kondratyev.[11] For the ground, the surface temperature ($T_g$) is used. Computation of Tg is described below.

The sensible heat flux density, H, is calculated by either of two methods: first, from measurements of profiles of wind speed and temperature made at several levels in the surface layer of the atmosphere; second, from the same kinds of measurements made at a single level in the surface layer. (The surface layer is that portion of the atmosphere directly above the ground and varies on the order of a few to a hundred meters in thickness depending upon the time of day. In this experiment, our meteorological measurements were made from the surface to a height of 8 meters.) In the first method, H is calculated from profile data by use of the empirical formulae of Businger et al.[12] The second method uses a simple formula originally developed by Burke.[13]

G pertains to heat flow in homogeneous material,

$$G = K \frac{\partial T}{\partial Z}. \tag{4}$$

Expressed as a finite difference, G is directly proportional to the quantity $T_1$ minus $T_g$, where $T_1$ is the first level below the surface ($T_1 = T(t, Z = 1)$).

The coupled set of equations, (2) and (3), are solved by numerical techniques. This is required because of the highly non-linear nature of the surface boundary condition. At t = 0, an initial temperature profile is specified. Equation (2) is solved by an explicit finite difference technique. A vertical grid in Z is used with 1 cm increments from the surface to 0.5 meter. The temperature for the next time step, t = 1, is then computed for each step in Z from the finite-difference approximation of (2),

$$T(t+1, Z) = T(t,Z) + \kappa \frac{\Delta t}{(\Delta Z)^2} \left[ T(t, Z+1) - 2T(t,Z) + T(t, Z-1) \right]. \tag{5}$$

The solution to (5) remains stable provided,

$$\kappa \left[ \frac{\Delta t}{(\Delta Z)^2} \right] < 0.5,$$

which limits the time steps, $\Delta t$, to 50 s or less. An updated value of the surface temperature is obtained by solving (3) in terms of $T_g$, i.e.

$$T\ (T+1,\ 0) = T_g, \tag{6}$$

so that a quartic equation in $T_g$ is obtained,

$$T_g^4 + C_1\ T_g + C_2 = 0, \tag{7}$$

where $C_1$ and $C_2$ are constants determined from S, R, H, and G. Equation (7) can be solved numerically by using the Newton-Raphson iterative technique. Finally, the solution is advanced in time by repeated application of this procedure until a complete set of temperature measurements is obtained as a function of depth and time. For a given set of environmental parameters, i.e. components of (3), and for a material with a known value of P (K, $\rho$, c), a unique set of surface temperature variations is predicted from the model.

In applying remote sensing techniques to geologic problems, it is not the surface temperature variations that need to be determined, but the thermal inertia. This requires inverting the numerical process described above. Once the diurnal temperature range ($\Delta T$) and the environmental parameters are given, the inversion proceeds in three stages: (1) the model is run for a range of thermal values, (2) a look-up table is generated which gives $\Delta T$ as a function of P, and (3) the table is inverted to give P as a function of $\Delta T$. The look-up table is, in this version of the model, really two-dimensional. In addition to $\Delta T$, the albedo is allowed to vary over the remotely sensed area so that P is actually a function of $\Delta T$ and albedo. On the other hand, meteorological conditions are assumed to be invariant with respect to surface locations. Topography also can be included as a surface variable (i.e. slope and slope azimuth) in the model which would result in a four dimensional look-up table. However, in the present study we have ignored the effects of topography. They will be included later.

The details of creating a photographic facsimile of a thermal inertia image are given in another paper.[8] In short, daytime and nighttime temperature images are made from thermal IR radiance data. The data are rectified to account for such systematic effects as camera optics, viewing geometry, and platform motion. Additionally, the data sets are registered vis-a-vis a suitable topographic map of the region so that a one-to-one correspondence can be achieved between recognizable features on both the map and the temperature images. A day-night temperature difference image, $\Delta T$, is then produced. The JPL thermal model is then applied to this data set, which includes albedo and environmental parameters.

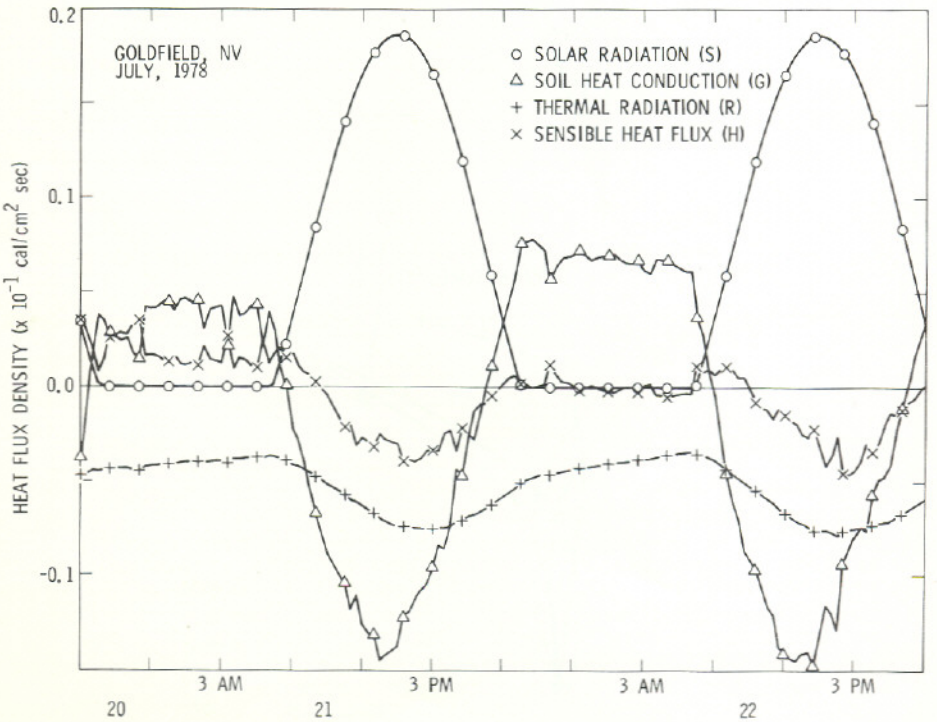


Figure 1. Surface heating processes.

## Results of a Field Test

The test site was located in the western Nevada desert in a region surrounding the town of Goldfield. The test period was in July, 1978; during this time, two consecutive overflights of HCMM occurred on the 22nd at 0230 and 1330 LT (local time). Field measurements at various locations were made of: (1) surface temperature with a Barnes PRT-5 radiation thermometer, (2) soil temperature profiles with Yellow Springs Instrument thermistor probes, and (3) meteorological conditions with the JPL micrometeorological mast[14] and a Meteorology Research Inc. mechanical weather station.

Figure 1 shows the components of equation (3) computed for the Goldfield area study. Sky conditions were mostly clear throughout the period. Wind speed and air temperature variations, at a height of 2 meters, were regular, with the range in air speeds about 1.0 to 7.0 m/s, and temperature about 10 to 37°C. The values of H calculated from these data by the method of Burke [13] show that the sensible heat flux carries heat away from the surface during the day and toward it at night. (Fluxes directed toward the surface are positive.) The solar radiation is the largest component, positive in the day and zero at night; the effect of the net thermal radiation is to cool the surface, day or night. The ground heat flux shows a wide variation: in the day, it augments the sensible heat flux and thermal radiation in their efforts to remove heat from the surface; at night, it counteracts the effect of radiative heat loss from the surface by transporting heat to the surface from the warmer layers below.

The soil temperature profile for a playa (dry-lake) south of Goldfield (Ralston area) is shown for six different times on the 21st (see Figure 2). These values are computed from the model and closely correspond to the observed values (see Figure 3). These curves illustrate how the diurnal temperature wave is damped with depth.

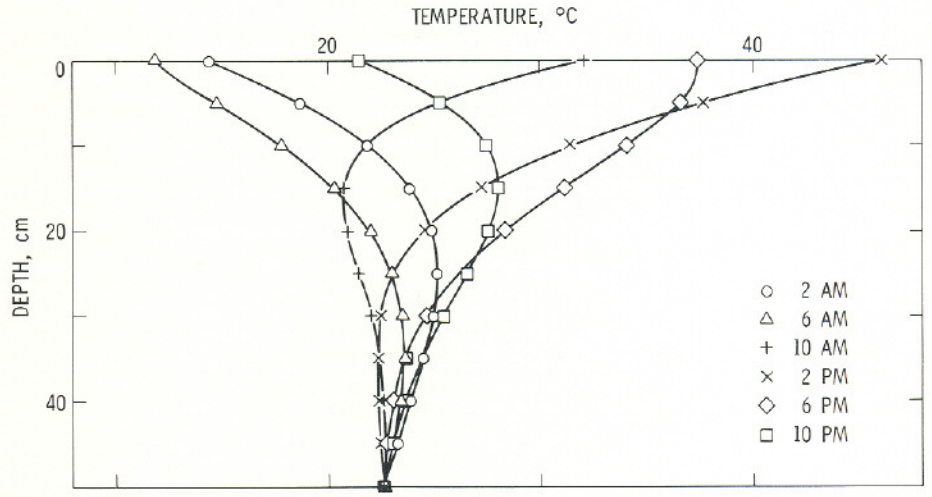


Figure 2. Soil temperature profiles, obtained from thermal model.

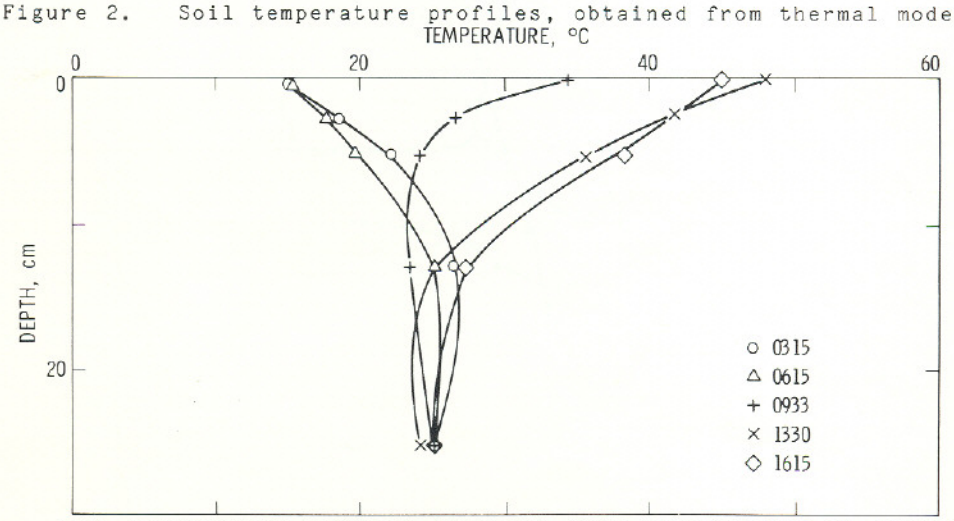


Figure 3. Soil temperature profiles obtained from measurements on Stonewall playa.

Based on the Goldfield meteorological data and model computations, the next set of Figures, 4 through 6, illustrates the soil temperature profile at 0600 and 1400 LT, and

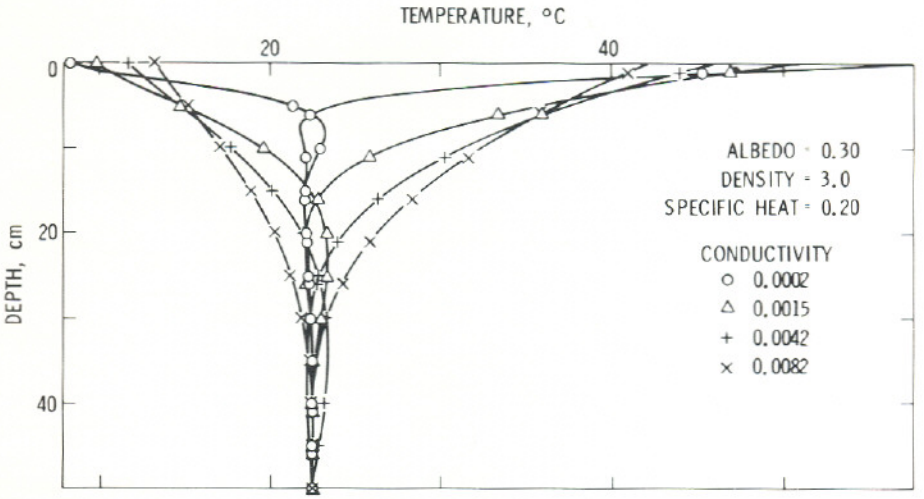


Figure 4. Soil temperature profiles obtained by varying thermal conductivity (cal/sec cm°C)

indicates how the near surface temperature range, ΔT, varies for different thermal properties. These curves were computed by varying each thermal property independently of the others while keeping the initial and boundary conditions invariant. In Figure 4, the conductivity is the variable. Increasing the conductivity, which results in increasing values of P, allows the diurnal heating wave to penetrate more deeply and results in decreasing ΔT at the surface. Figures 5 and 6 show that increasing either the specific heat

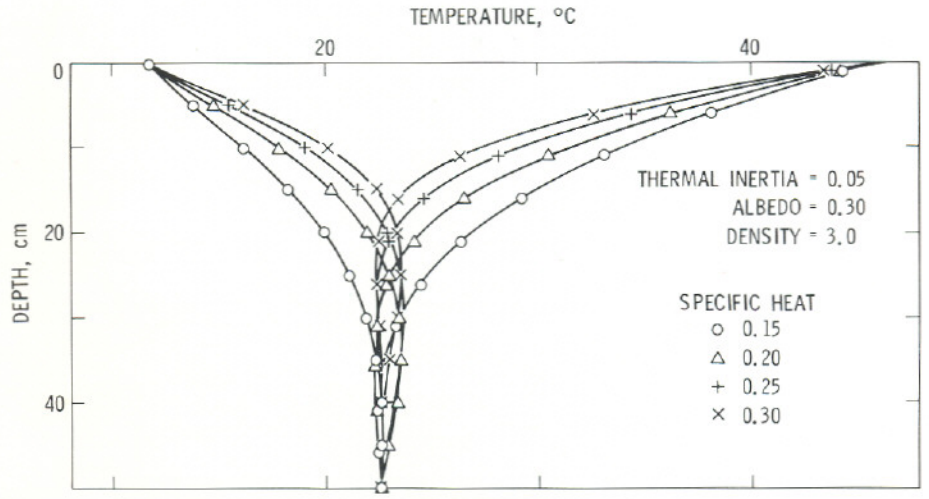


Figure 5. Soil temperature profiles obtained by varying specific heat (cal/gm°C).

or the density, concentrates the heating in the near surface layers at the expense of the soil at lower depths. These curves indicate the importance of thermal inertia in identifying geologic materials by remote sensing techniques, since the surface temperature is the only thermal property that can be measured in this way. This is depicted graphically in Figure 7 which shows the surface temperature variation as a function of thermal inertia. Increasing P reduces the diurnal temperature range. Furthermore, it does not matter what combination of K, ρ, c produces a given P value. Doubling K, or reducing ρ or c by half, affects the way heat is distributed throughout the soil layer but that is not manifested in the surface temperature history. Since P is the same, the diurnal surface temperation variations will be the same.

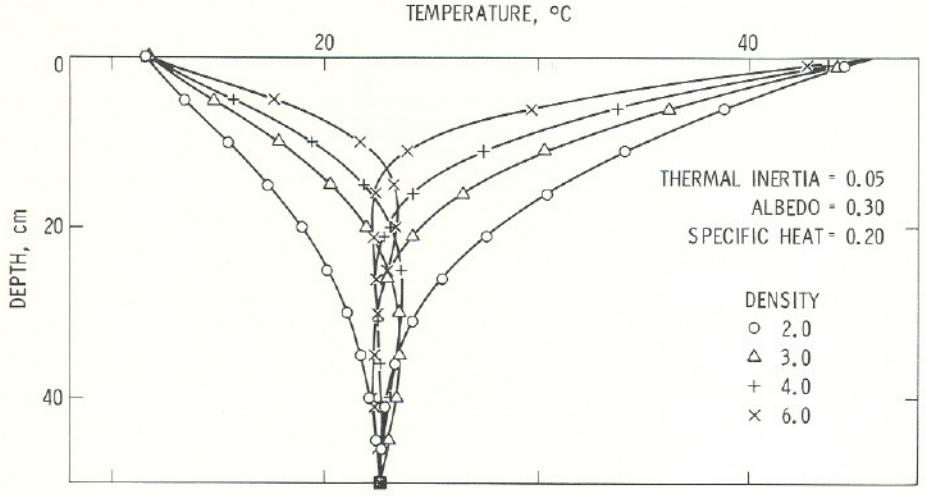


Figure 6. Soil temperature profiles obtained by varying density ($gm/cm^3$).

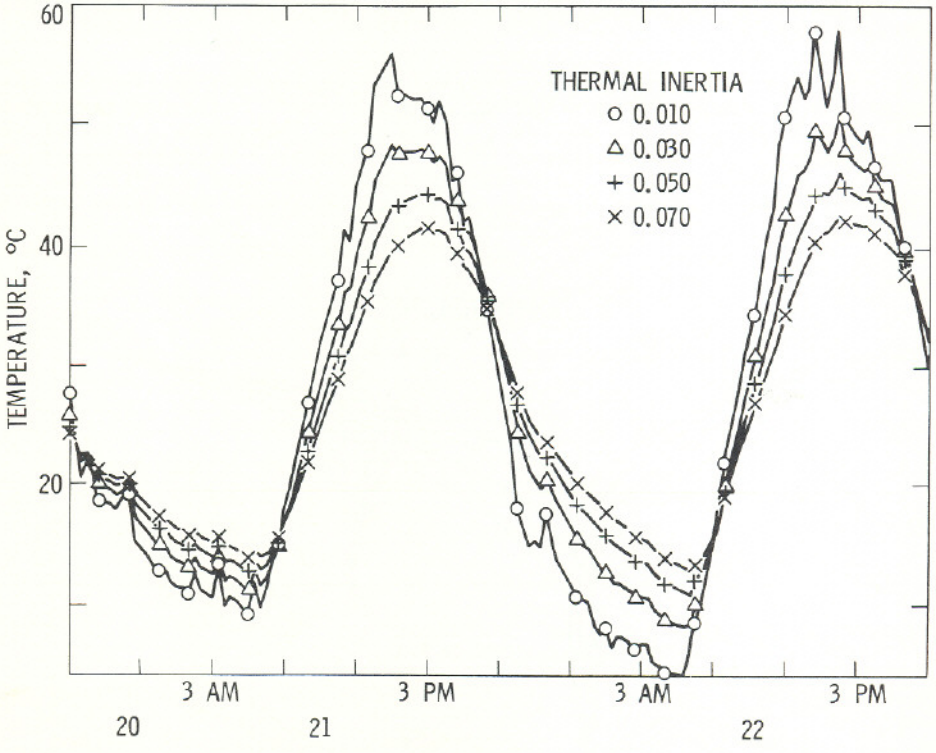


Figure 7. Surface temperature variation as a function of thermal inertia.

Finally, with these considerations in mind, we show two images of the Goldfield area for comparison. Figure 8 shows albedo and Figure 9 computer-derived thermal inertia. Prominent landmarks are labeled for reference. These are indicated by capital letters: (C) is the Clayton Valley area which includes sand dunes, a large oblong-shaped playa, and a body of standing water located on the playa; (M) is Mud Lake, a large playa; (G) is the town of Goldfield; (S) is Stonewall Mountain, whose tallest peak is about 2480 m high; (R) is a finger-shaped playa (the bright spot below R on the albedo image) in the Ralston area. On the thermal image, altered rocks are denoted by the lower case letter a. In Figure 9, light areas denote high thermal inertia values and dark areas low values. The light area in the upper left-hand corner (C) is a large area of standing water on a playa. Isolated bright dots and associated dark spots are clouds and their shadows. Much of the thermal inertia pattern can be ascribed to topography. Nevertheless, one important difference between the albedo and thermal inertia images is in the discrimination between hydrothermally altered rocks and unaltered ones at essentially the same elevation.[15] The

albedo image shows no clear distinction between the two rock types, whereas the altered rocks are seen as light patches (high thermal inertia) on the thermal inertia image. (The distribution of altered rocks is indicated by the short, white lines radiating from the indicator, a.)

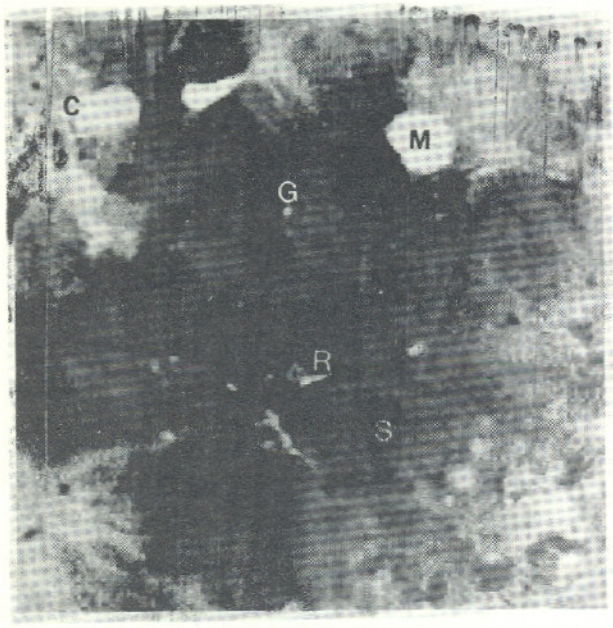


Figure 8. Albedo image of Goldfield, NV area.

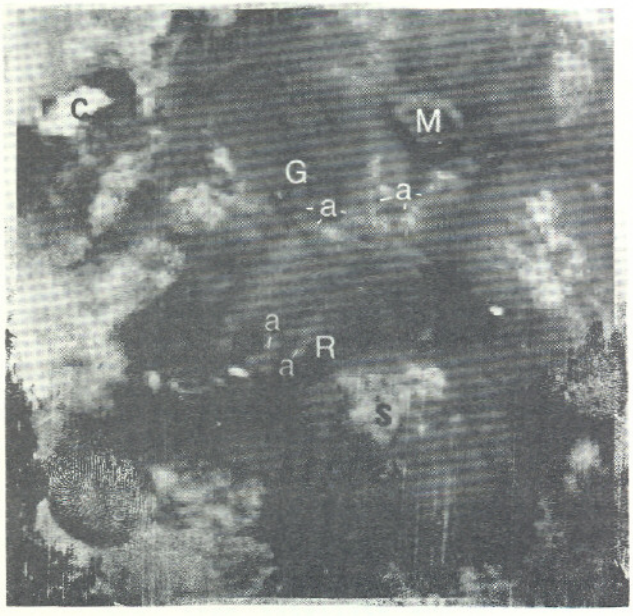


Figure 9. Thermal inertia images of the same area.

## Conclusions

These preliminary results indicate thermal inertia images can be useful tools in separation of some geologic materials by remote sensing techniques. Furthermore, they form a valuable set of complementary data for use with other types of remote sensing measurements. Despite the successful results indicated here, there remains a host of problems to be solved if this technique is to be widely applicable. These include refinements in obtaining surface meteorological measurements; ideally, they should be derivable from either synoptic weather data or meteorological satellite measurements. Moreover, the considerable horizontal variability in meteorological conditions, that usually exists on a mesoscale, is not accounted for in this model. Other features that need inclusion are

atmospheric attenuation of the IR signal, topography, vegetation effects, non-uniform soil layers, and soil moisture transport. Finally, while the results shown here indicate one successful application of HCMM data to geology, the extent of the general class of geologic problems where these data will be useful has yet to be investigated. Many of these problems are now the subjects of current investigations.

## Acknowledgment

This paper is the result of research carried out at the Jet Propulsion Laboratory, California Institute of Technology, under Contract NAS7-100 sponsored by the National Aeronautics and Space Administration

## References

1. Kahle, A. B., A. R. Gillespie, and A. F. H. Goetz, "Thermal Inertia Imaging: A New Geologic Mapping Tool," Geophys. Res. Lett., Vol 3, pp. 26-28. 1976.

2. Jaeger, J. C., "Conduction of Heat in a Solid With Periodic Boundary Conditions, with an Application to the Surface Temperature of the Moon," Proc. Cambridge Phil. Soc., Vol. 49 (2), pp. 355-359. 1953.

3. Watson, K., A Computer Program of Thermal Modeling for Interpretation of Infrared Images, Rep. PB 203578, 33 pp., U.S. Geol. Surv., Washington, D.C. 1971.

4. Watson, K., "Periodic Heating of a Layer Over a Semi-Infinite Solid," J. Geophys. Res., Vol. 78, pp. 5904-5910. 1973.

5. Rosema, A., A Mathematical Model for Simulation of the Thermal Behavior of Bare Soils, Based on Heat and Moisture Transfer, Publ. 11, Neth. Interdepartmental Work, Community for the Appl. of Remote Sensing Tech., Delft, Netherlands. 1975.

6. Kahle, A. B., "A Simple Thermal Model of the Earth's Surface for Geologic Mapping by Remote Sensing," J. Geophys. Res., Vol. 82, pp. 1673-1680. 1977.

7. Price, J. C., "Heat Capacity Mapping Mission," J. Brit. Interp. Soc., Vol. 31, pp. 313-316. 1978.

8. Gillespie, A. R. and A. B. Kahle, "Construction and Interpretation of a Digital Thermal Inertia Image," Photogramm. Eng. Remote Sensing, Vol. 43, pp. 983-1000. 1977.

9. Joseph, J. H., "On the Calculation of Solar Radiation Fluxes in the Troposphere," Solar Energy, Vol. 13, pp. 251-261. 1971.

10. Arakawa, A., A. Katayama, and Y. Mintz, Numerical Simulation of the General Circulation of the Atmosphere, Proc. WMO/IUGG Symp. on Numerical Weather Prediction, Tokyo. 1968.

11. Kondratyev, K. Ya., Radiation in the Atmosphere, Academic Press. 1969.

12. Businger, J. A., J. C. Wyngaard, Y. Izumi, and E. F. Bradley, "Flux-Profile Relationships in the Atmospheric Surface Layer," J. Atmos. Sci., Vol. 28, pp. 181-189. 1971.

13. Burke, C. J., "Transformation of Polar Continental Air to Polar Maritime Air," J. of Meteor., Vol. 2, pp. 94-112. 1945.

14. Kahle, A. B., J. Schieldge, and H. Paley, JPL Field Measurements at the Finney County, Kansas, Test Site, October 1976: Meteorological Variables, Surface Reflectivity, Surface and Subsurface Temperatures, JPL Pub. 77-1. 1977.

15. Rowan, L. C., A. F. H. Goetz, and R. P. Ashley, "Discrimination of Hydrothermally Altered and Unaltered Rocks in Visible and Near Infrared Multispectral Images," Geophysics, Vol. 42, pp. 522-535. 1977.